BBA - Molecular Basis of Disease 1864 (2018) 3247–3256

Contents lists available at ScienceDirect

BBA - Molecular Basis of Disease

journal homepage: www.elsevier.com/locate/bbadis

Tau localises within mitochondrial sub-compartments and its caspase cleavage affects ER-mitochondria interactions and cellular Ca^{2+} handling

Domenico Cieri[a,1], Mattia Vicario[a,1], Francesca Vallese[a], Beatrice D'Orsi[a], Paola Berto[a], Alessandro Grinzato[a], Cristina Catoni[b], Diego De Stefani[a], Rosario Rizzuto[a], Marisa Brini[b], Tito Calì[a,c,*]

[a] Department of Biomedical Sciences, University of Padova, Padova, Italy
[b] Department of Biology, University of Padova, Padova, Italy
[c] Padova Neuroscience Center (PNC), University of Padova, Padova, Italy

ARTICLE INFO

Keywords:
Tau
Mitochondria
ER-mitochondria contact sites
SPLICS
Mitochondrial sub-compartments

ABSTRACT

Intracellular neurofibrillary tangles (NFT) composed by tau and extracellular amyloid beta (Aβ) plaques accumulate in Alzheimer's disease (AD) and contribute to neuronal dysfunction. Mitochondrial dysfunction and neurodegeneration are increasingly considered two faces of the same coin and an early pathological event in AD. Compelling evidence indicates that tau and mitochondria are closely linked and suggests that tau-dependent modulation of mitochondrial functions might be a trigger for the neurodegeneration process; however, whether this occurs either directly or indirectly is not clear. Furthermore, whether tau influences cellular Ca^{2+} handling and ER-mitochondria cross-talk is yet to be explored. Here, by focusing on wt tau, either full-length (2N4R) or the caspase 3-cleaved form truncated at the C-terminus (2N4RΔC_{20}), we examined the above-mentioned aspects. Using new genetically encoded split-GFP-based tools and organelle-targeted aequorin probes, we assessed: i) tau distribution within the mitochondrial sub-compartments; ii) the effect of tau on the short- (8–10 nm) and the long- (40–50 nm) range ER-mitochondria interactions; and iii) the effect of tau on cytosolic, ER and mitochondrial Ca^{2+} homeostasis. Our results indicate that a fraction of tau is found at the outer mitochondrial membrane (OMM) and within the inner mitochondrial space (IMS), suggesting a potential tau-dependent regulation of mitochondrial functions. The ER Ca^{2+} content and the short-range ER-mitochondria interactions were selectively affected by the expression of the caspase 3-cleaved 2N4RΔC_{20} tau, indicating that Ca^{2+} mis-handling and defects in the ER-mitochondria communications might be an important pathological event in tau-related dysfunction and thereby contributing to neurodegeneration. Finally, our data provide new insights into the molecular mechanisms underlying tauopathies.

1. Introduction

Intracellular tau neurofibrillary tangles (NFTs) and extracellular formation of Aβ-plaques represent key pathologic hallmarks of Alzheimer's disease (AD) [1,2]. NFTs have been found in neurons of the entorhinal cortex and the hippocampus. The increase in NTFs levels within the brain clinically correlates with dementia [3,4]. Tau, a highly soluble microtubule-associated protein (MAP) that promotes their assembly and stabilisation, is the main constituent of NTFs [5]. Post-translational modifications, including truncation, hyper-phosphorylation and conformational changes, are at the basis of tau-mediated pathology [6]. In the fibrillar pathologies of AD, caspase 3 cleavage of tau at Asp421 occurs before the nuclear events of apoptosis [7] and generates a truncated protein that aggregates more rapidly due to a conformational change induced by the lack of its basic C-terminal 20 amino acids. Under physiological conditions, this C-terminal domain inhibits tau filament assembly [8], possibly by self-association with the acidic N-terminal projection domain, which is also involved in the interaction with other cytoskeletal elements, including mitochondria or neuronal plasma membrane [9–11]. Truncated tau associates with both early and late NFTs markers and its presence correlates with cognitive decline [1,12,13]. Additionally, truncated tau is aberrantly phosphorylated and its caspase-mediated cleavage is an early event that may precede hyper-phosphorylation [7]. Tau hyper-phosphorylation is indeed a common

* Corresponding author at: Department of Biomedical Sciences, University of Padova, Padova, Italy.
E-mail address: tito.cali@unipd.it (T. Calì).
[1] Equal contribution.

https://doi.org/10.1016/j.bbadis.2018.07.011
Received 28 March 2018; Received in revised form 16 June 2018; Accepted 6 July 2018
Available online 11 July 2018
0925-4439/

feature of the neurofibrillary changes that occur in all tauopathies [14]. There are six different isoforms of tau in the adult human brain, 0 N, 1 N or 2 N with 3R or 4R [15]. They differ on the number of the 29-residue near-N-terminal insert (N) encoded by exons 2 and 3, and depending on whether they contain three or four C-terminal repeat domains (R; the second of which is encoded by exon 10). The tau sequence contains several phosphorylation sites that, in AD patients' brain, undergo hyperphosphorylation and aggregation in paired helical filaments (PHF) [16]. The phosphorylation state of tau has an impact on the functional state of the protein, affecting both its binding to microtubules and its aggregation properties. Tau accumulation triggers a cascade of events that eventually leads to its propagation from cell to cell in a prion-like mode, spreading tauopathy to other areas of the brain [17]. Despite the importance of tau modifications in the aetiology of AD has been well described, how it affects cellular function and leads to neurodegeneration is still unclear. Mitochondrial alterations were demonstrated in transgenic mice overexpressing tau protein and mice injected with tau oligomers [18,19]. The expression of wt (2N4R) or caspase 3-cleaved tau (2N4RΔC_{20}; able to induce fibrillation and seeding of wt tau as well [20,21]) has been reported to cause perinuclear clustering of mitochondria [22–25] and changes in mitochondrial shaping proteins expression levels [22,23] in fibroblasts from sporadic AD patients, rat hippocampal neurons as well as several mammalian cell lines, suggesting an intimate relationship between mitochondria and tau.

Tau overexpression increases retrograde mitochondrial transport, whereas it decreases complex I activity and ATP levels [23]. Mitophagy deficits and changes in mitochondrial membrane potential were reported both in *in vitro* and *in vivo* models for tau accumulation [27], and alterations of mitochondrial trafficking were detected in the axon of sensory neurons of zebrafish embryos expressing mutant tau and in cells expressing different forms of tau [28,29]. Thus, mitochondria might be an important route through which tau leads to the degeneration and death of specific subsets of neuronal cells. Nevertheless, whether these events occur as a consequence of tau-induced dysfunctions that fall back on mitochondria or can be directly triggered by tau at mitochondrial level is still unclear. Some evidence supporting the localisation of tau (wt, phosphorylated form or caspase cleaved N-terminal fragment) within mitochondria or its association with the OMM has recently emerged [18,27,30,31] and suggested the intriguing possibility that “mitochondrial” tau may also play a role in the cellular dysfunctions found in tauopathies. In the present study, we investigated the localisation of tau at mitochondria and within sub-mitochondrial compartments by employing a novel and improved split-GFP based bimolecular fluorescence complementation (BiFC) methodology [32,33]. This tool was originally developed by us to selectively monitor DJ-1 sub-mitochondrial distribution [34]. In addition to the previously described OMM- and matrix-targeted $GFP_{1–10}$ [34], a new IMS targeted non-fluorescent $GFP_{1–10}$ moiety has been generated to selectively track protein translocation within the IMS. Two different tau constructs were C-terminally tagged with the GFP beta strand 11 (β_{11}): one encoding the wt full-length tau (2N4R) and the other one encoding the C-terminally deleted tau at position 421 (2N4RΔC_{20}). 2N4RΔC_{20} expression has been shown to induce mitochondrial fragmentation, increase of reactive oxygen species, reduction in mitochondrial motility and decrease of Ca^{2+} buffering capacity upon thapsigargin treatment [26,35–37]. The GFP-moieties-fused proteins were employed to specifically monitor and quantify tau distribution at the OMM, IMS and mitochondrial matrix. We also evaluated whether tau expression could result in Ca^{2+} signalling alterations. To this end, we assessed the consequences of tau 2N4R and 2N4RΔC_{20} overexpression on cytosolic, ER and mitochondrial Ca^{2+} homeostasis using organelle targeted aequorin-luminescent probes [38]. Lastly, we estimated the tau-dependent effect on ER-mitochondria interactions by the quantification of the number of short- (8–10 nm) and long- (40–50 nm) range contacts, [39], using a novel probe that we have recently developed. Hence, we detected constitutive presence of tau at the OMM and in the IMS, but not in the mitochondrial matrix. Moreover, we observed that caspase 3-cleaved tau, typically found in the brain of patients with mild cognitive impairment stage of AD [7,20] and associated with the formation of tau aggregates, affects ER Ca^{2+} levels and short-, but not long-, range ER-mitochondria interactions. These data suggest that tau may directly participate in the pathophysiology of mitochondria-related activities by interfering with ER-mitochondria communication, reinforcing the concept that an early involvement of mitochondrial dysfunctions, Ca^{2+} dyshomeostasis and ER-mitochondria Ca^{2+} cross-talk impairment might have a role in the pathogenesis of AD.

2. Materials and methods

2.1. DNA constructs

The full length hTau WT-β_{11} construct (2N4R) has been generated by PCR using the following primers: FL-hTau WT-S11 (*Bam*HI) For 5′-ATAAGTTCGGATCCATGGCTGAGCCCCGCCAGGAGTTCG-3′; FL-hTau WT-S11(*Xho*I) Rev. 5′-ACTTCTCACTCGAGTCATGTGATGCCGGC GGCGTTCACGTACTCGTGCAGCACCATGTGGTCCCGGCTGCCGCCGCC GCTGCCGCCGTCGCCCAAACCCTGCTTCGCGAGGGAGGCAG-3′. The ΔC_{20} hTau-β_{11} construct (2N4RΔC_{20}) has been amplified by PCR using the FL-hTau WT-S11 (*Bam*HI) For primer and the ΔC_{20}-S11 (*Xho*I) Rev. 5′-ACTTCTCACTCGAGTCATGTGATGCCGGCGGCGTTCACGTACTCGTG CAGCACCATGTGGTCCCGGCTGCCGCCGCCGCTGCCGCCGTCGCCGTC TACCATGTCGATGCTGCCGGTGG-3′. The DNA construct encoding for the human tau in pcDNA3, used as a template, was a kind gift of Dr. Paolo Paganetti (Laboratory for Biomedical Neurosciences, Neurocenter of Southern Switzerland). The β_{11} tagged Cytochrome-*c* at the C-terminus was produced by DNA synthesis (Thermo Scientific). The $GFP_{1–10}$ targeted to the intermembrane space (IMS) has been created by genetic fusion to the leader sequence of the IMS protein LACTB [40,41] and created by DNA synthesis (Thermo Scientific). To specifically monitor ER-mitochondria interactions with the newly generated split-GFP based sensor (SPLICS), the untagged versions of each tau constructs were generated introducing a stop codon before the β_{11} tag by site-direct mutagenesis. All constructs were confirmed by sequencing.

2.2. Cell culture and transfection

HeLa cells were grown in DMEM high glucose medium (Euroclone) supplemented with 10% Fetal bovine serum (FBS, GIBCO), 100 U/ml penicillin (Euroclone) and 100 μg/ml streptomycin (Euroclone).

For immunocytochemistry and contacts quantification, cells were seeded onto 13 mm glass coverslips, whereas for western blotting and Ca^{2+} measurements onto 6-multiwell plates, and allowed to grow to 60–80% confluence. Transfection was carried out 12 h after seeding with the Ca^{2+} phosphate procedure using 5 μg of total DNA for each 13 mm glass coverslip and 12 μg for each well of the 6-multiwell plate. For Ca^{2+} measurements, cells were co-transfected with Aequorin constructs targeted to different cell compartments (mtAEQ, cytAEQ and erAEQ) and pcDNA3 empty vector (control) or tau FL-hTau WT and ΔC_{20} with a 1:2 ratio in favour of tau. For ER-mitochondria contact sites quantification, HeLa cells were co-transfected with $SPLICS_S$ (short range contacts) or $SPLICS_L$ (long range contacts) in combination with void vector or FL-hTau WT or ΔC_{20} in a 1,5:1,5:2 ratio in favour of the overexpressed protein.

2.3. Preparation of post-natal mouse neocortical neurons

Primary cultures of cortical neurons were prepared from post-natal days 0–2. To isolate the cortical neurons, mouse pups were euthanized by cutting their heads off with large scissors. The cerebral cortices were isolated from each pup and pooled in a dissection medium on ice (PBS with 0.25% glucose, 0.3% bovine serum albumin [BSA]). The tissue was incubated with 0.25% trypsin-EDTA at 37 °C for 15 min. After the

incubation, the trypsinisation was stopped by the addition of fresh plating medium (minimal essential medium [MEM] containing 5% fetal bovine serum, 5% horse serum, 100 U/ml penicillin/streptomycin [Pen/Strep], 0.5 mM L-glutamine, 0.6% D-glucose). The neurons were then dissociated by gentle pipetting and after centrifugation (1500 rpm, 3 min), the medium containing trypsin was aspirated. Neocortical neurons were resuspended in plating medium, plated at 2×10^5 cells per cm^2 on poly-D-lysine-coated plates (final concentration of 5 μg/ml), and then incubated at 37 °C and 5% CO_2. The plating medium was exchanged with 50% feeding medium (NBM-embryonic containing 100 U/ml of Pen/Strep, 2% B27 and 0.5 mM L-glutamine), 50% plating medium with additional mitotic inhibitor cytosine arabinofuranoside (600 nM). Two days later the medium was again exchanged for complete feeding medium. Neocortical neurons (days in vitro, DIV 5) were transfected using Lipofectamine 2000 (Invitrogen) and stainings were performed on DIV 7.

2.4. Calcium measurements

Ca^{2+} concentration measurements were carried out in a Perkin-Elmer Envision plate reader equipped with a two-injector unit. Twenty-four hours after transfection, cells were plated onto a 96-well plate. The day after, recombinant wt cytAEQ or mutant mtAEQ were reconstituted by incubating HeLa cells for 1,5 h with 5 μM wt coelenterazine (Santa Cruz Biotechnology) in modified Krebs Ringer Buffer (KRB: 125 mM NaCl, 5 mM KCl, 400 mM KH2PO4, 1 mM $MgSO_4$, 20 mM Hepes, pH 7.4) supplemented with 5 mM glucose at 37 °C. To functionally reconstitute low affinity ER targeted aequorin, the ER Ca^{2+} content was drastically reduced by incubating cells for 1,5 h at 4 °C with KBR supplemented with 5 μM of the Ca^{2+} ionophore ionomycin (Sigma), 600 μM EGTA and 5 μM coelenterazine n (Biotium). Cells were then washed with KRB supplemented with 2% bovine serum albumin (Sigma) and 1 mM EGTA. After reconstitution, cells were placed in 70 μl of KRB supplemented as indicated in the figures and luminescence from each well was measured for the indicated period of time. According to the experiment, Ca^{2+} transients were generated by the addition of 100 μM histamine (Sigma) or 2 mM $CaCl_2$ at the final concentration. The experiments were terminated by lysing the cells with 100 μM digitonin (Sigma) in a hypotonic Ca^{2+}-rich solution (10 mM $CaCl_2$ in H_2O) to discharge the remaining reconstituted aequorin pool. Output data were analysed and calibrated with a custom made macro-enabled Excel workbook.

2.5. Western blot analysis

36 h after transfection, HeLa cells were processed for western blot analysis. Cells were washed with ice-cold PBS and solubilised in ice-cold lysis buffer (150 mM NaCl, 50 mM Tris-HCl, pH 7.4, 10 mM EGTA/Tris, pH 7.4, 1% Triton X-100) containing 1 mM protease inhibitors cocktail (Sigma). Postnuclear supernatants were collected after 10 min of centrifugation at 10,000 *g* at 4 °C. The total protein content was determined by the Bradford assay (Bio-Rad). Samples were loaded on a 15% SDS-PAGE Tris/HCl gel, transferred onto PVDF membranes (Merck Millipore), blocked for 1 h with 5% milk in TBS-T (Tris Buffered Saline-Tween, 20 mM Tris, 0.137 M NaCl, pH 7.6, 0.1% Tween 20) at 4 °C and incubated overnight with a mouse monoclonal antibody recognizing all tau isoforms (Anti-tau 4-repeat isoform RD4, clone 1E1/A6, Merck Millipore), and mouse monoclonal anti β-Actin (Sigma), mouse polyclonal anti Tom20 (Santa Cruz) or tubulin (Santa Cruz) as endogenous control (dilutions are 1:1000). Detection was carried out by incubation with secondary horseradish peroxidase-conjugated anti-mouse IgG antibody (Santa Cruz) for 1 h at room temperature and proteins were visualized by the chemiluminescent reagent Luminata Western HRP substrate (Merck Millipore).

2.6. Cellular fractionation

Cells were plated on a Petri dish and transfected with 30 μg of total DNA. 36 h after transfection cells were washed with PBS and harvested using a scraper. Cells were then collected in a tube, centrifuged at 1400 rpm for 4 min at 4 °C, washed with 10 mM Hepes supplemented with 0.25 M sucrose and resuspended in 500 μl of the same solution. Cells were then lysate using a potter and centrifuged 10 min at 1000 *g* to pellet nuclei. 50 μl of the supernatant were collected and used as total lysate (PNS: post-nuclear supernatant). The remaining supernatant was centrifuged at 10,000 *g* for 6 min to pellet mitochondria. The resulting supernatant (cytosol) was collected and lysed by adding 1% Triton X-100. Both mitochondria and cytosol were washed and centrifuged 5–6 times with Hepes supplemented with sucrose (dealing with the cytosol, each time 20 μl of lysate were left in the tube to dilute contamination with other cellular fractions). Mitochondria were resuspended in 300 mM NaCl, 10 mM $CaCl_2$, 100 mM Tris HCl pH 8.5 and 0.5% NP40 for 30 min at 4 °C.

2.7. Immunocytochemistry analysis

36 h after transfection, HeLa cells were stained for immunofluorescence. The cells were washed twice with PBS (140 mM NaCl, 2 mM KCl, 1.5 mM KH_2PO_4, 8 mM Na_2HPO_4, pH 7.4), fixed for 20 min in 3.7% formaldehyde (Sigma) and washed three times with PBS. The cells were then permeabilised in 0.1% Triton X-100 in PBS, followed by a 1 h wash with 1% gelatin (type IV, from calf skin) (Sigma) in PBS. Cells were then incubated for 1 h at 37 °C in a wet chamber with a mouse monoclonal antibody recognizing all tau isoforms (Anti-tau 4-repeat isoform RD4, clone 1E1/A6, Merck Millipore) or with a rabbit polyclonal anti-Tom20 antibody (Santa Cruz Biotechnology) at a 1:20 dilution in PBS. Staining was performed with Alexa Fluor 488 or 633-labeled anti-mouse or Alexa Fluor 594 anti-rabbit secondary antibody (Molecular Probes, Carlsbad, CA) at a 1:50 dilution in PBS.

36 h post transfection, cortical neurons grown on 13-mm coverslips and transfected with the different constructs were loaded with the MitoTracker Mitochondrion-selective probe Red (Invitrogen, 200 nM) for 30 min. Following incubation time, neurons were washed once in PBS and fixed with 4% paraformaldehyde for 15 min, permeabilised in PBS containing 0.1% Triton X-100 and washed three times with PBS. For nuclear staining, Hoechst 33258 (Sigma; 1 μg/ml) was then added into the wells for 30 min, after which coverslips were then transferred to glass slides with a mounting medium and sealed around the edges with clear varnish. Images were acquired with a Leica SP5 inverted confocal microscope and analysed by ImageJ software.

2.8. Quantification of biFC at the IMS

To quantify biFC at the IMS, a complete z-stack of cells showing a clear fluorescence signal was acquired using a Leica SP5 confocal microscope. The total corrected cell fluorescence (TCCF) was calculated as previously described [42]. Briefly, the selected cell was outlined using the freehand selection of Fiji and the remaining signal coming from outside the cell was removed. Area, integrated density and mean grey value were then measured within the cells and three selected non-fluorescent area in the image were chosen as background. The TCCF was calculated as follow: integrated density – (area of selected cell × mean fluorescence of background readings). The calculated TCCF was then normalised against the TCCF values of wt tau-expressing cells. The results are shown as fold change increase/decrease over 2N4R-tau expressing cells TCCF levels.

2.9. Mitochondrial distribution analysis

To quantify mitochondrial distribution within the cell, we used the Radial Profile Plot plugin available on Fiji (https://imagej.nih.gov/ij/

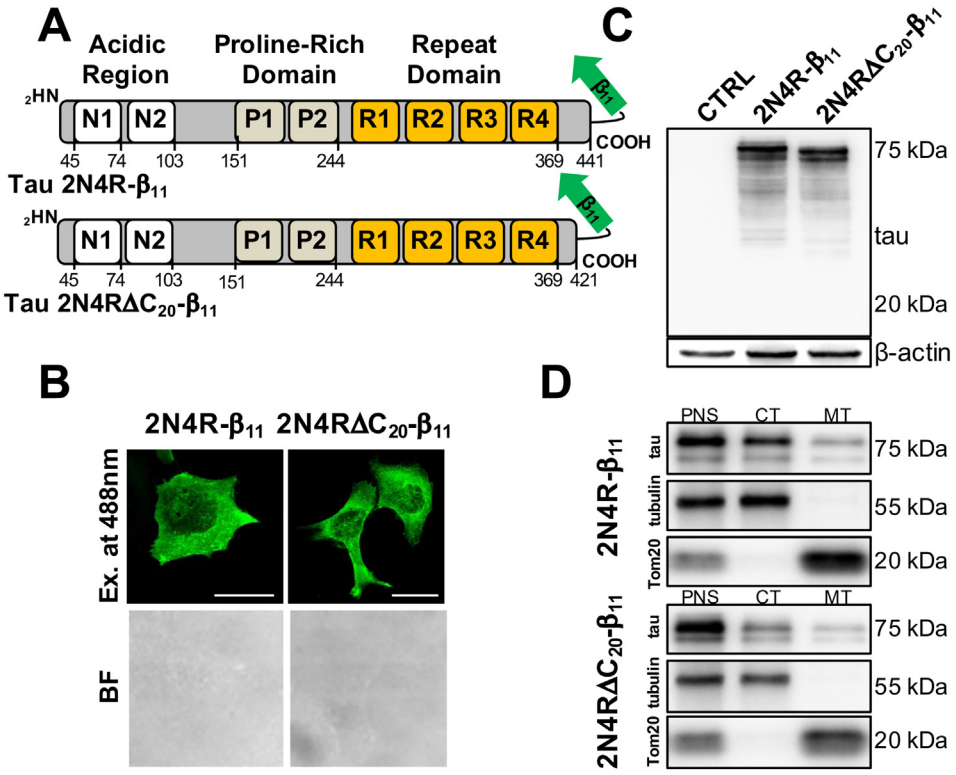

Fig. 1. Tau-β_{11} expression in HeLa cells. (A) Schematic representation of the different tau forms expressed in HeLa cells. The C-terminally-fused β_{11} fragment is depicted in green. (B) Representative confocal images of tau-β_{11} transfected HeLa cells immunostained with an anti-tau antibody. Scale bar = 25 μm. (C) Western blot from total cell lysates showing tau-β_{11} expression levels in HeLa cells. The membrane was incubated with a tau antibody and β-actin was used as loading control. (D) Western blot from cellular fractionation of tau transfected cells and empty vector control showing tau in the different cellular compartments. Tubulin and Tom20 were employed as markers of the cytosolic and mitochondrial fraction, respectively. PNS: Post-nuclear supernatant, CT: cytosol; MT: mitochondria. (For interpretation of the references to color in this figure legend, the reader is referred to the web version of this article.)

plugins/radial-profile.html). The plugin analyses the distribution of normalised integrated intensities around concentric circles starting from a specific point: in our case, the nucleus of the cell, set manually by drawing a circle. The distribution of fluorescence intensities was analysed on a radius of 200–300 pixels, sufficient to cover, on most cases, the overall area occupied by the cell. Spatial calibration was used to measure the maximal distance occupied by mitochondria in microns: for each cell, the first value of "Normalised Integrated Intensity" above 0.1 was considered as the most distant point in which mitochondria could be detected (Max. Radius in the graph in Fig. 2C).

2.10. ER-mitochondria contact sites quantification

48 h after transfection, HeLa cells were excited at 488nm and analysed by using a Leica TSC SP5 inverted microscope equipped with a HCX PL APO 100×/numerical aperture 1.4 oil immersion objective. A complete z-stack of each cell was captured every 0.29 μm with the Leica AS software. To quantify inter-organelle contact sites, images were processed using Fiji software. Images were convolved, filtered with Gaussian Blur and reconstructed in three dimensions using the Volume J plugin. A selected face of the 3D rendering was then thresholded and used to count ER-mitochondria contacts.

2.11. Statistical analysis

Results shown are mean values ± SEM. Student's unpaired two-tailed *t*-test was used for comparisons involving two groups when sample followed a Gaussian distribution. Differences between groups were considered significant when $p \leq 0.05$. All statistical analyses were performed using GraphPad Prism version 6.00 for Mac OS X, GraphPad Software (La Jolla, California, USA). The exact values of n and their means are indicated in the text. $^{*}p \leq 0.01$, $^{**}p \leq 0.0005$, $^{***}p \leq 0.0001$.

3. Results

3.1. Tau localises to mitochondria

In order to verify tau mitochondrial localisation, we employed split GFP-based tools and generated two constructs encoding two variants of human wt tau tagged with the GFP-β_{11} at their C-terminus (Fig. 1A): the full-length tau containing 4 repeats (2N4R-β_{11}) and a truncated tau form at position 421 (2N4RΔC_{20}-β_{11}). The tau-encoding constructs were transfected in HeLa cells and their expression and subcellular localisation were assessed by immunocytochemistry and western blot analysis. Anti-tau antibody staining showed a diffused distribution of the protein within the cell (Fig. 1B). Western blots on total lysates from HeLa cells transfected with the different constructs confirmed their correct expression at the expected molecular weights (Fig. 1C). Similar results were obtained with the untagged human tau constructs (Fig. S1), demonstrating that the expression and subcellular localisation of the protein were not altered by the addition of the β_{11} fragment at their C-terminus. We next performed subcellular fractionation experiments on HeLa cells transfected with the human tau-β_{11} constructs and observed their localisation within mitochondria. As shown in Fig. 1D, the 2N4R-β_{11} protein, corresponding to the wt full-length tau, was found in the post nuclear supernatant fraction (PNS) and in the cytosolic fraction (CT), as expected. Interestingly, the crude mitochondrial fraction (MT) also contained the protein, as previously observed [23,27,31,43]. Analogously, the 2N4RΔC_{20}-β_{11} tau was detected in PNS and CT fractions and, surprisingly, in the mitochondrial fraction as well. The purity of the fractionation experiment was verified by probing the blotting membrane with specific antibodies against proteins of the cytosol (tubulin) and mitochondria (Tom20). Altogether, these data suggest that under basal conditions a fraction of the cellular tau is associated to mitochondria. Whether the tau fraction at mitochondrial level has a physiological meaning or represents a product of degradation of this "fibrillogenic" protein is still unknown.

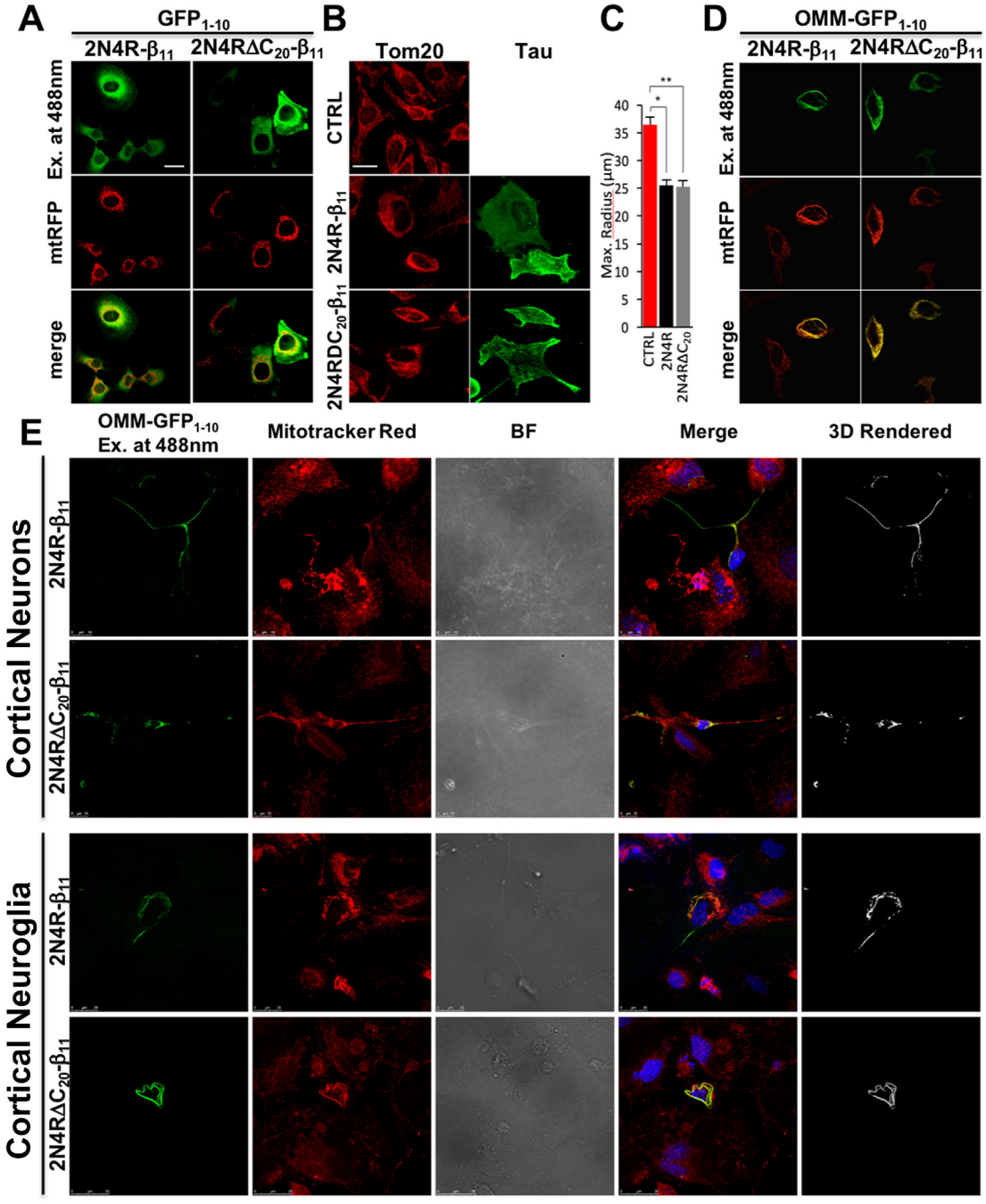

Fig. 2. Cytosolic and outer mitochondrial membrane distribution of tau revealed by GFP biFC and tau-induced mitochondrial alterations. The interaction between tau-β_{11} and the different $GFP_{1–10}$ fragments results in biFC that is detected as a fluorescent signal. (A) Confocal pictures showing HeLa cells co-transfected with tau-β_{11}, cytosolic $GFP_{1–10}$ and mitochondrial RFP (mtRFP). (B) Confocal images showing mitochondrial distribution in control and tau-transfected HeLa cells. Mitochondria and tau were immunostained with an anti-Tom20 (red) and anti-tau (green) antibody, respectively. (C) Histogram representing mitochondrial distribution in HeLa cells upon the conditions shown in B. (D) GFP biFC was used to analyse tau localisation at the outer mitochondrial membrane. Co-transfection of HeLa cells with 2N4R-β_{11}, the 2N4RΔC_{20}-β_{11} tau and OMM-$GFP_{1–10}$ resulted in GFP biFC at the OMM that co-localised with the mitochondria-targeted pTagRFP-mito plasmid. The merge of the GFP biFC and the mitochondrial signal are shown on the right. (E) Confocal imaging showing the OMM localisation of tau in mouse primary cortical neurons (top) and non-neuronal cells, mainly neuroglia (bottom). Scale bar = 25 μm. (For interpretation of the references to color in this figure legend, the reader is referred to the web version of this article.)

3.2. A split-GFP based approach to reveal tau distribution within the mitochondria

To better identify tau function at the mitochondrial level, it was necessary to define its presence in the different sub-mitochondrial compartments. Despite cellular fractionation clearly showed tau association with mitochondria, this technique does not allow to discriminate in which specific compartment it is distributed. To address this aspect, we exploited the split-GFP based approach, developed and successfully employed by our group, to selectively assess the sub-mitochondrial localisation of the PD-related protein DJ-1 [34]. This technique is based on the ability of the super folder GFP variants, namely the $GFP_{1–10}$ (GFP without an essential β-strand) and the β_{11} (the lacking β-strand required for the reconstitution of the chromophore), to

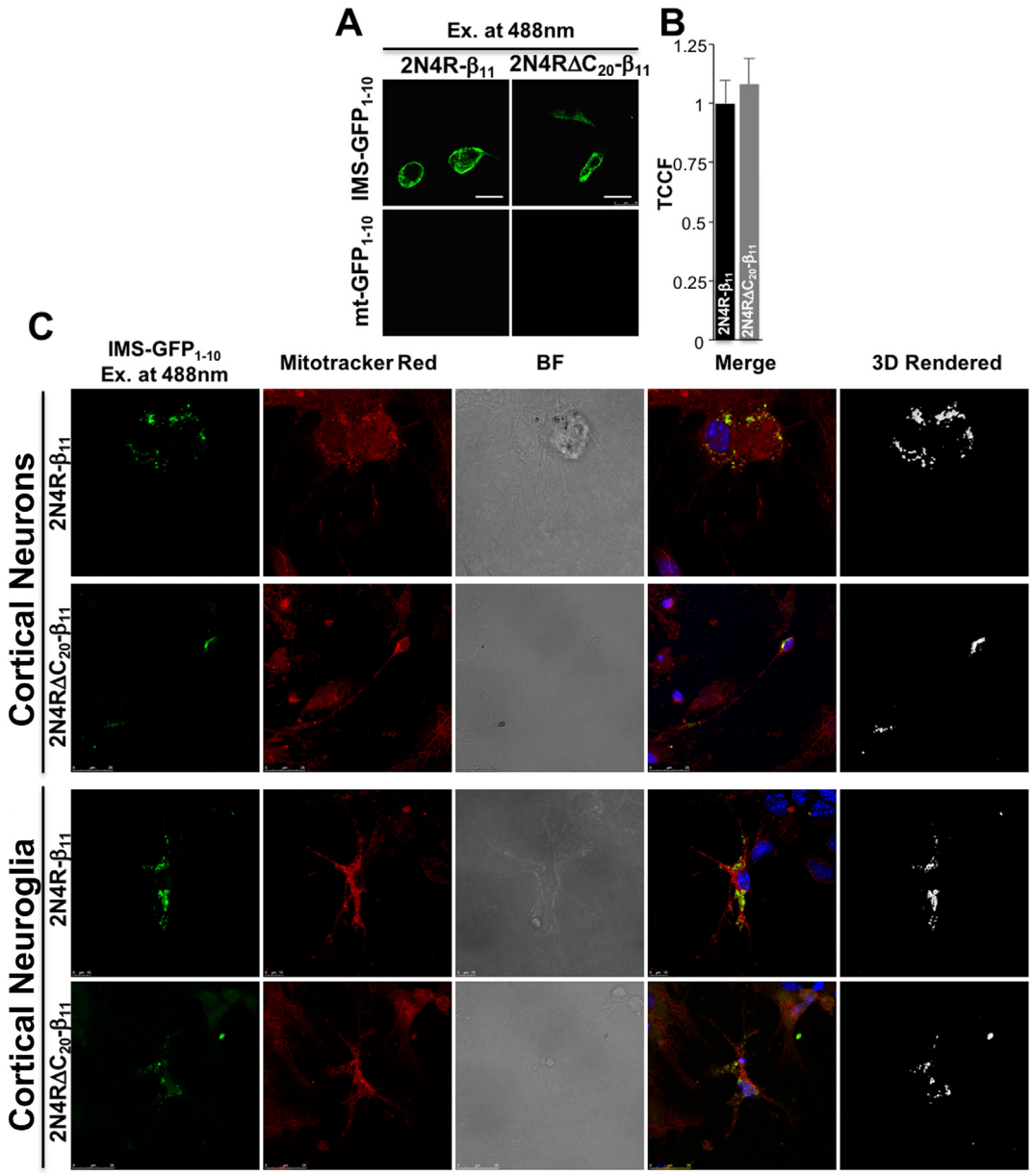

Fig. 3. Sub-mitochondrial distribution of tau revealed by GFP biFC. (A) GFP biFC was used to analyse tau localisation at the inter membrane space (top) and (bottom) mitochondrial matrix. (B) Histogram showing the quantification of the GFP biFC signal detected with the IMS-GFP$_{1–10}$ fragment. (D) Confocal images showing the IMS localisation of tau in mouse primary cortical neurons (top) and non-neuronal cells, mainly neuroglia (bottom). Scale bar = 25 μm.

self-assemble and, thus, reconstitute the GFP fluorescence [32,33]. In addition to the previously described GFP$_{1–10}$ constructs targeted to either the outer mitochondrial membrane (OMM-GFP$_{1–10}$) or the mitochondrial matrix (mt-GFP$_{1–10}$) [44], we have now expanded and completed the palette of constructs available to detect protein localisation/translocation within all the mitochondrial sub-compartments by developing a novel GFP$_{1–10}$ construct targeted to the intermembrane space (IMS-GFP$_{1–10}$). First, we verified whether the proper self-assembly of the newly generated GFP fragments efficiently occurred also in the IMS by co-transfecting HeLa cells with IMS-GFP$_{1–10}$ and a β_{11}-tagged cytochrome-*c* constructs. Fig. S2 clearly documented the appearance of a mitochondrial signal that perfectly co-localises with a mitochondrialtargeted RFP. To assess whether and where the β_{11} tau constructs were able to assemble and reconstitute GFP fluorescence, we initially co-transfected them in HeLa cells together with an untargeted cytosolic GFP$_{1–10}$. The resulting diffused fluorescence pattern (Fig. 2A) confirmed that GFP reconstitution mainly occurred in the cytosol, where the β_{11} tau proteins were detected by immunocytochemistry analysis (Fig. 1B). Interestingly, we noticed that, upon the expression of either 2N4R-β_{11} and 2N4RΔC$_{20}$-β_{11} tau, mitochondria appeared fused and mostly distributed at the perinuclear region (see mtRFP signal in Fig. 2A). To explore in more detail this aspect, we labeled mitochondria with an anti-Tom20 antibody to evaluate their distribution both in controls and in cells expressing 2N4R or 2N4RΔC$_{20}$ tau. In control cells, mitochondria occupied most of the cell area, spreading from the perinuclear region to cell periphery (Fig. 2B, top panel, CTRL). On the contrary, 2N4R and 2N4RΔC$_{20}$ tau expression conferred a peculiar cell phenotype: mitochondria were largely concentrated at the perinuclear region and excluded from cell periphery, as previously reported [23,24] (Fig. 2B, middle and bottom panels). Quantification of the radial distribution of mitochondria from the center of the cell confirmed this observation (Fig. 2C, max. radius values (μm): 36,51 ± 2,4 n = 15 for control cells; 25,49 ± 1,17 n = 16 for 2N4R-β_{11}; 25,22 ± 1,73 n = 18 for 2N4RΔC$_{20}$-β_{11}). These results also suggested that the C-terminal 20

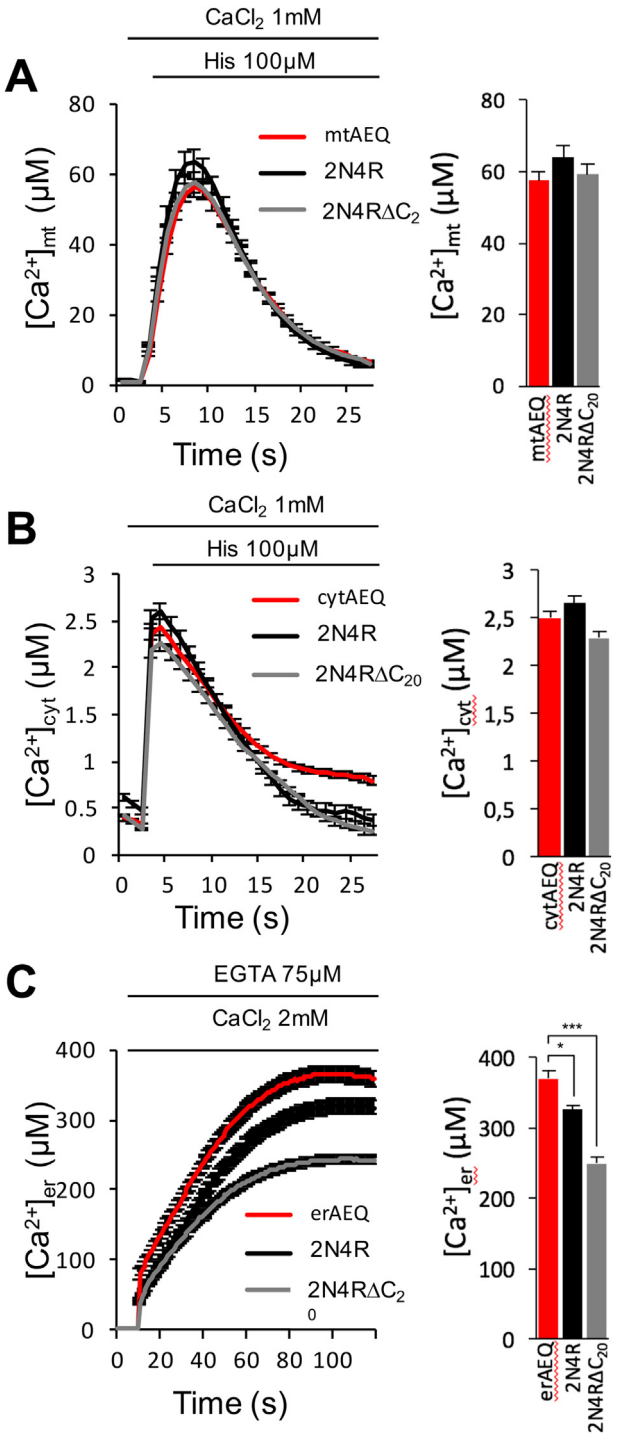

Fig. 4. Ca^{2+} handling in HeLa cells overexpressing the tau constructs. Ca^{2+} was measured in the different compartments by using mitochondrial (A), cytosolic (B) or ER-targeted (C) Aequorin. Ca^{2+} transients are shown on the left, whereas average Ca^{2+} peaks on the right.

amino acids of tau are dispensable for the observed effect on mitochondrial distribution.

To investigate in which specific sub-mitochondrial compartment tau localises and/or translocates, 2N4R-β_{11} and 2N4RΔC_{20}-β_{11} tau constructs were separately co-transfected in HeLa cells along with different $GFP_{1–10}$ plasmids targeted to either the OMM, IMS or the mitochondrial matrix. Fluorescence reconstitution at mitochondrial level is expected to take place only in the compartments where tau is effectively present. As shown in Fig. 2D, co-expression of either the 2N4R-β_{11} and 2N4RΔC_{20}-β_{11} constructs with the OMM-$GFP_{1–10}$ fragment led to a green fluorescence signal, which is fully overlapping with that of the mitochondrial marker, mtRFP. Of note, the GFP-reconstituted signal revealed strong mitochondrial fusion and, although we could not exclude that the GFP reconstitution might drive part of cytosolic tau to concentrate at the mitochondrial surface and/or affect its dissociation from the OMM, suggests that tau accumulation at the OMM might be important for the regulation of the mitochondrial fission/fusion. Tau localisation at the OMM and the above-mentioned effects on mitochondrial morphology were also confirmed in a more complex cellular system, i.e., in mouse primary cortical neurons (Fig. 2E, top panels) as well as in non-neuronal cells, mainly neuroglia, present, in small percentage, in the post-natal neuronal culture (Fig. 2E, bottom panels).

Analogously, to verify whether tau localises in the IMS and/or the mitochondrial matrix, the β_{11}-tagged tau constructs were co-transfected in HeLa cells with the IMS-$GFP_{1–10}$ or the mt-$GFP_{1–10}$ fragments (Fig. 3A). 2N4R-β_{11} and 2N4RΔC_{20}-β_{11} tau constructs were able to reconstitute the GFP fluorescence within the IMS (upper panel), indicating that a fraction of the two tau forms was present there. We have also quantified the total corrected cell fluorescence (for details, see materials and methods section) and found that the abundance of the two tau constructs within the cell was similar (Fig. 3B; TCCF values: 1 ± 0,09 n = 26 for 2N4R-β_{11}; 1,08 ± 0,1 n = 29 for 2N4RΔC_{20}-β_{11}). When the tau constructs were co-expressed with the mt-$GFP_{1–10}$ probe targeted to the mitochondrial matrix, we could not detect any specific mitochondria-localised signal, suggesting that none of the tested tau forms localised to this sub-compartment (bottom panel). We have also verified the presence of tau at the IMS in mouse cortical neurons (Fig. 3C, top panels) as well as in non-neuronal cells (Fig. 3C, bottom panels). As shown in the figure, a strong fluorescence was detected upon co-expression of the β_{11}-tagged tau constructs along with the IMS targeted $GFP_{1–10}$, suggesting that a fraction of tau was present at the level of the IMS also in these cells.

Altogether, these data showed that, under physiological conditions, a fraction of tau localises both at the OMM and in the IMS, and that tau affects mitochondrial morphology independently from its C-terminal 20 amino acids.

3.3. Effect of tau expression on cell Ca^{2+} handling and ER-mitochondrial interactions

The detection of tau at the OMM and the IMS prompted us to examine mitochondrial parameters that may be affected by tau expression. Thus, we monitored Ca^{2+} homeostasis and ER-mitochondria interactions in the short- (8–10 nm) and long- (40–50 nm) range using the newly generated split-GFP based sensors (SPLICS) [39]. Because the β_{11}-tagged tau constructs interfere with SPLICS reconstitution, we used their untagged versions for the evaluation of ER-mitochondria contact sites.

Firstly, we employed organelle-targeted aequorin probes to analyse Ca^{2+}-handling in specific cellular compartments, i.e., mtAEQmut for the mitochondrial matrix, cytAEQ for the cytoplasm and erAEQ for the ER lumen [38]. Considering the effects of tau expression on mitochondrial morphology, we initially assessed the ability of mitochondria to take up Ca^{2+} upon cell stimulation with the $InsP_3$-linked agonist histamine. The expression of both 2N4R and 2N4RΔC_{20} tau did not result in an altered mitochondrial Ca^{2+} handling (Fig. 4A. peak values: 57.58 ± 2.3 n = 30 for control cells; 63.87 ± 3.23 n = 32 for 2N4R-β_{11}; 59.24 ± 2.7 n = 31 for 2N4RΔC_{20}-β_{11}). Similarly, no differences were observed in cytosolic Ca^{2+} transients generated by histamine stimulation (Fig. 4B. peak values: 2.49 ± 0.07 n = 32 for control cells; 2.65 ± 0.07 n = 32 for 2N4R-β_{11}; 2.28 ± 0.07 n = 32 for 2N4RΔC_{20}-β_{11}), suggesting that the expression of wt and truncated tau did not affect bulk cellular Ca^{2+} handling.

However, both 2N4R and 2N4RΔC_{20} tau overexpression decreased

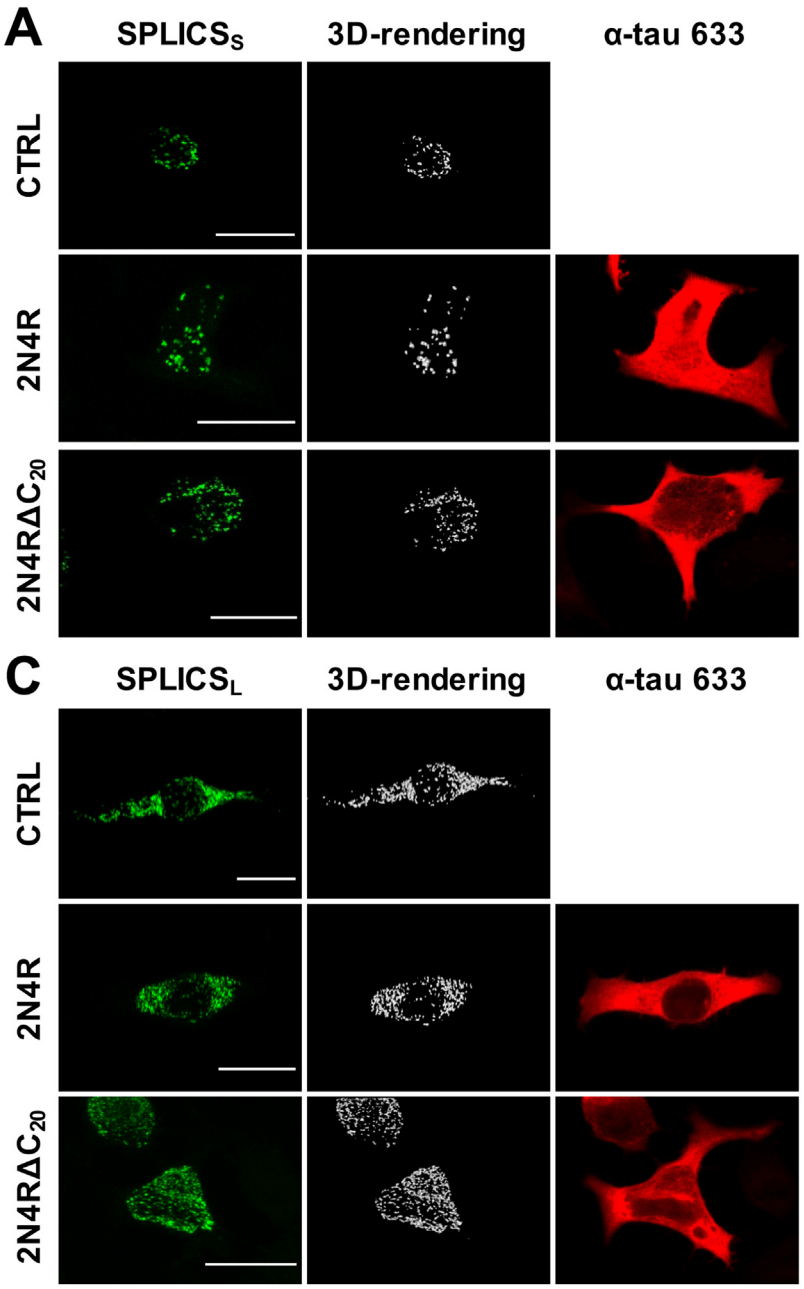

Fig. 5. Effects of tau expression on ER-mitochondria contact sites. Immunofluorescence against tau (red) is shown on the right, whereas ER-mitochondria contact sites detected with the SPLICS on the left (green). (A) Representative confocal images of HeLa cells expressing the SPLICS$_S$ probe. (B) Quantification of the SPLICS$_S$ contact sites number by 3D rendering of complete z-stacks. (C) Representative confocal images of HeLa cells expressing the SPLICS$_L$ probe. (D) Quantification of the SPLICS$_L$ contact sites number by 3D rendering of complete z-stacks. Scale bar = 25 μm. (For interpretation of the references to color in this figure legend, the reader is referred to the web version of this article.)

the steady-state ER Ca^{2+} content, as the caspase-cleaved tau form is more effective than the wt level (Fig. 4C. plateau values: 370.62 ± 11.64 $n = 20$ for control cells; 326.29 ± 6.44 $n = 22$ for 2N4R-β_{11}; 249.31 ± 9.29 $n = 24$ for 2N4RΔC_{20}-β_{11}).

Because the observed reduction in ER Ca^{2+} content did not result in a diminished mitochondrial Ca^{2+} transients, we hypothesised that the ER-mitochondria connection may be affected by tau expression and, in particular, by the 2N4RΔC_{20} mutant. The coupling between ER and mitochondria is indeed fundamental for ER-mitochondria Ca^{2+} transfer; in fact, this transfer and the correct proximity between the two organelles is regulated by several proteins, some of which have been involved in familial forms of neurodegenerative diseases [45]. To date, only one study reported a possible relationship between tau protein and ER-mitochondria tethering, showing that the number of contacts between mitochondria and RER membranes is increased in motor neurons derived from JNPL3 mice overexpressing P301L mutant tau compared to their controls [46]. Interestingly, this study also confirmed the presence of tau at mitochondria by EM analysis. We therefore quantified the number of ER-mitochondria contact sites in our cell models and discriminated their nature using SPLICS approach recently developed in our laboratory [39]. Indeed, the development of the two versions of SPLICS (SPLICS$_S$ or SPLICS$_L$) not only highlighted the heterogeneity in the ER-mitochondria contact sites, but also unravelled their differential modulation upon different cellular conditions [39]. Both short (8–10 nm) and long- (40–50 nm) range ER-mitochondria interactions were measured in HeLa cells transfected with SPLICS$_S$ or SPLICS$_L$ in the absence and in the presence of 2N4R and 2N4RΔC_{20} tau. As shown in Fig. 5A (and quantified in Fig. 5B), the expression of 2N4RΔC_{20}, but not of the full-length 2N4R tau, significantly increased the number of the tight ER-mitochondria interactions (number of ER-mitochondria contacts/cell: 67.83 ± 5.03 $n = 31$ for control cells; 71.55 ± 6.11 $n = 27$ for 2N4R-β_{11}; 120.42 ± 11.12 $n = 28$ for 2N4RΔC_{20}-β_{11}). On the other hand, long range ER-mitochondria contacts sites were not affected in both cases (Fig. 5C and quantification in 5D; number of ER-mitochondria contacts/cell: 198.07 ± 8.24 $n = 26$ for control cells; 174.7 ± 9.85 n = 27 for 2N4R-β_{11}; 190.64 ± 11.52 $n = 25$ for

2N4RΔC$_{20}$-β$_{11}$). The increased juxtaposition between the two organelles observed in the presence of 2N4RΔC$_{20}$ tau may serve to mitigate the reduction in the [Ca^{2+}]$_{er}$ (Fig. 4C), possibly to keep unaltered mitochondrial Ca^{2+}-transients (Fig. 4A) and, thus, to guarantee a proper ER-mitochondrial Ca^{2+} transfer to efficiently cope with the bioenergetic demand of the cell.

4. Discussion

Increasing evidence links tau to impaired mitochondrial functions [47]. Full-length tau, as well as the caspase-3 cleaved form 2N4RΔC$_{20}$, were detected at the mitochondrial level, suggesting the intriguing possibility that several mitochondria-related functions may be directly influenced by tau at this site [18,27,30,31]. Nevertheless, due to the lack of tools to unequivocally establish its distribution in the sub-mitochondrial compartments, the role of tau at the mitochondrial level is still not clear and essentially unexplored. Furthermore, whether and how tau may affect the formation/stabilisation of the contact sites between the ER and mitochondria, in turn impacting on the ER and mitochondrial Ca^{2+} uptake, is largely unknown. Using a split-GFP based approach, we here showed that GFP fluorescence reconstitution occurs upon co-expression of either the 2N4R-β$_{11}$ or 2N4RΔC$_{20}$-β$_{11}$ constructs with the OMM-GFP$_{1–10}$ and the IMS-GFP$_{1–10}$ fragments, but not with the mtGFP$_{1–10}$, demonstrating the presence of a tau faction both at the OMM and the mitochondrial IMS, and its absence in the mitochondrial matrix. Under basal conditions, the tau presence in these sub-compartments suggests that the protein might exert important functions locally, by acting on targets at the OMM (e.g., OPA1 and mitofusins, including Mfn1, Mfn2) [23]) and/or in the IMS. Indeed, we have found that, also in our conditions, tau expression affects mitochondrial distribution. Additional experiments are required to better understand how and why tau localises at these sub-mitochondrial compartments, nevertheless it is tempting to consider the possibility that it is related to the cytosolic proteostasis maintenance mechanism through the import of misfolded/aggregation prone proteins into mitochondria [48]. Although under basal conditions we did not detect tau in the mitochondrial matrix, we cannot exclude its translocation there under specific conditions, as previously demonstrated for the PD-related protein DJ-1 [34].

A strong reduction of the ER Ca^{2+} content was observed in cells expressing the 2N4RΔC$_{20}$ truncation form of tau. This decrease is accompanied by a strong enhancement in the short-range ER-mitochondria contact sites, suggesting potential compensatory mechanisms able to maintain the correct ER-mitochondria Ca^{2+} transfer. Indeed, mitochondrial Ca^{2+} transients were similar to control cells. Regarding wt tau, the modest, but statistically significant, reduction in the ER Ca^{2+} content was probably not enough to be compensated by an increase in the short-range ER-mitochondria associations, suggesting that only the caspase-3 cleaved form of tau selectively impacts on the ER-mitochondria axis possibly through a ER Ca^{2+} mishandling mechanism. This might be due to a direct effect on the ER Ca^{2+} handling machinery, such as the SERCA pump, the IP_3R or indirectly via an ER stress response triggered by the 2N4RΔC$_{20}$ mutant tau. However, further experiments would be required to better understand and clarify this hypothesis. At present, we cannot establish whether the reduction of ER Ca^{2+} level or the increase in ER-mitochondrial tethering occurs first; however, we can conclude that tau accumulation interferes with this key signalling, a feature shared with other proteins linked to neurodegenerative diseases such as Presenilin2, α-synuclein or VAPB/PTPIP51 [49–51].

Supplementary data to this article can be found online at https://doi.org/10.1016/j.bbadis.2018.07.011.

Transparency document

The Transparency document associated this article can be found, in online version.

Acknowledgements

We would like to thank Prof. Paola Pizzo and Dr. Riccardo Filadi (Department of Biomedical Sciences, University of Padova) for critically reading the manuscript and for helpful suggestions. We also thank Dr. Paolo Paganetti (Laboratory for Biomedical Neurosciences, Neurocenter of Southern Switzerland, Switzerland) for kindly providing the tau expression vector. The work is supported by grants from the Ministry of University and Research (Bando SIR 2014 n° RBSI14C65Z to T.C.) and from the Università degli Studi di Padova (Progetto Giovani 2012 n° GRIC128SP0 to T.C., Progetto di Ateneo 2016 n° CALI_SID16_01 to T.C. and Progetto di Ateneo 2015 n° CPDA153402 to M.B.).

Conflict of interest

The authors declare that they have no conflicts of interest with the contents of this article.

References

[1] I. Grundke-Iqbal, K. Iqbal, Y.C. Tung, M. Quinlan, H.M. Wisniewski, L.I. Binder, Abnormal phosphorylation of the microtubule-associated protein tau (tau) in Alzheimer cytoskeletal pathology, Proc. Natl. Acad. Sci. U. S. A. 83 (1986) 4913–4917.
[2] I. Grundke-Iqbal, K. Iqbal, L. George, Y.C. Tung, K.S. Kim, H.M. Wisniewski, Amyloid protein and neurofibrillary tangles coexist in the same neuron in Alzheimer disease, Proc. Natl. Acad. Sci. U. S. A. 86 (1989) 2853–2857.
[3] A.C. McKee, K.S. Kosik, N.W. Kowall, Neuritic pathology and dementia in Alzheimer's disease, Ann. Neurol. 30 (1991) 156–165.
[4] P.V. Arriagada, J.H. Growdon, E.T. Hedley-Whyte, B.T. Hyman, Neurofibrillary tangles but not senile plaques parallel duration and severity of Alzheimer's disease, Neurology 42 (1992) 631–639.
[5] M.D. Weingarten, A.H. Lockwood, S.Y. Hwo, M.W. Kirschner, A protein factor essential for microtubule assembly, Proc. Natl. Acad. Sci. U. S. A. 72 (1975) 1858–1862.
[6] Y. Wang, E. Mandelkow, Tau in physiology and pathology, Nat. Rev. Neurosci. 17 (2016) 5–21.
[7] T.C. Gamblin, F. Chen, A. Zambrano, A. Abraha, S. Lagalwar, A.L. Guillozet, M. Lu, Y. Fu, F. Garcia-Sierra, N. Lapointe, R. Miller, R.W. Berry, L.I. Binder, V.L. Cryns, Caspase cleavage of tau: linking amyloid and neurofibrillary tangles in Alzheimer's disease, Proc. Natl. Acad. Sci. U. S. A. 100 (2003) 10032–10037.
[8] A. Abraha, N. Ghoshal, T.C. Gamblin, V. Cryns, R.W. Berry, J. Kuret, L.I. Binder, C-terminal inhibition of tau assembly in vitro and in Alzheimer's disease, J. Cell Sci. 113 (Pt 21) (2000) 3737–3745.
[9] D. Jung, D. Filliol, M. Miehe, A. Rendon, Interaction of brain mitochondria with microtubules reconstituted from brain tubulin and MAP2 or TAU, Cell Motil. Cytoskeleton 24 (1993) 245–255.
[10] R. Brandt, J. Leger, G. Lee, Interaction of tau with the neural plasma membrane mediated by tau's amino-terminal projection domain, J. Cell Biol. 131 (1995) 1327–1340.
[11] J. Al-Bassam, R.S. Ozer, D. Safer, S. Halpain, R.A. Milligan, MAP2 and tau bind longitudinally along the outer ridges of microtubule protofilaments, J. Cell Biol. 157 (2002) 1187–1196.
[12] M. Novak, J. Kabat, C.M. Wischik, Molecular characterization of the minimal protease resistant tau unit of the Alzheimer's disease paired helical filament, EMBO J. 12 (1993) 365–370.
[13] Y. Kim, H. Choi, W. Lee, H. Park, T.I. Kam, S.H. Hong, J. Nah, S. Jung, B. Shin, H. Lee, T.Y. Choi, H. Choo, K.K. Kim, S.Y. Choi, R. Kayed, Y.K. Jung, Caspase-cleaved tau exhibits rapid memory impairment associated with tau oligomers in a transgenic mouse model, Neurobiol. Dis. 87 (2016) 19–28.
[14] M.L. Billingsley, R.L. Kincaid, Regulated phosphorylation and dephosphorylation of tau protein: effects on microtubule interaction, intracellular trafficking and neurodegeneration, Biochem. J. 323 (Pt 3) (1997) 577–591.
[15] G. Lee, N. Cowan, M. Kirschner, The primary structure and heterogeneity of tau protein from mouse brain, Science 239 (1988) 285–288.
[16] M. Goedert, M.G. Spillantini, N.J. Cairns, R.A. Crowther, Tau proteins of Alzheimer paired helical filaments: abnormal phosphorylation of all six brain isoforms, Neuron 8 (1992) 159–168.
[17] M. Goedert, M. Masuda-Suzukake, B. Falcon, Like prions: the propagation of aggregated tau and alpha-synuclein in neurodegeneration, Brain 140 (2017) 266–278.
[18] C.A. Lasagna-Reeves, D.L. Castillo-Carranza, U. Sengupta, A.L. Clos, G.R. Jackson, R. Kayed, Tau oligomers impair memory and induce synaptic and mitochondrial dysfunction in wild-type mice, Mol. Neurodegener. 6 (2011) 39.
[19] D.C. David, S. Hauptmann, I. Scherping, K. Schuessel, U. Keil, P. Rizzu, R. Ravid, S. Drose, U. Brandt, W.E. Muller, A. Eckert, J. Gotz, Proteomic and functional analyses reveal a mitochondrial dysfunction in P301L tau transgenic mice, J. Biol. Chem. 280 (2005) 23802–23814.

[20] R.A. Rissman, W.W. Poon, M. Blurton-Jones, S. Oddo, R. Torp, M.P. Vitek, F.M. Laferla, T.T. Rohn, C.W. Cotman, Caspase-cleavage of tau is an early event in Alzheimer disease tangle pathology, J. Clin. Invest. 114 (2004) 121–130.
[21] J.J. Jarero-Basulto, J. Luna-Munoz, R. Mena, Z. Kristofikova, D. Ripova, G. Perry, L.I. Binder, F. Garcia-Sierra, Proteolytic cleavage of polymeric tau protein by caspase-3: implications for Alzheimer disease, J. Neuropathol. Exp. Neurol. 72 (2013) 1145–1161.
[22] X. Wang, B. Su, H. Fujioka, X. Zhu, Dynamin-like protein 1 reduction underlies mitochondrial morphology and distribution abnormalities in fibroblasts from sporadic Alzheimer's disease patients, Am. J. Pathol. 173 (2008) 470–482.
[23] X.C. Li, Y. Hu, Z.H. Wang, Y. Luo, Y. Zhang, X.P. Liu, Q. Feng, Q. Wang, K. Ye, G.P. Liu, J.Z. Wang, Human wild-type full-length tau accumulation disrupts mitochondrial dynamics and the functions via increasing mitofusins, Sci. Rep. 6 (2016) 24756.
[24] W. Stoothoff, P.B. Jones, T.L. Spires-Jones, D. Joyner, E. Chhabra, K. Bercury, Z. Fan, H. Xie, B. Bacskai, J. Edd, D. Irimia, B.T. Hyman, Differential effect of three-repeat and four-repeat tau on mitochondrial axonal transport, J. Neurochem. 111 (2009) 417–427.
[25] K.J. Kopeikina, G.A. Carlson, R. Pitstick, A.E. Ludvigson, A. Peters, J.I. Luebke, R.M. Koffie, M.P. Frosch, B.T. Hyman, T.L. Spires-Jones, Tau accumulation causes mitochondrial distribution deficits in neurons in a mouse model of tauopathy and in human Alzheimer's disease brain, Am. J. Pathol. 179 (2011) 2071–2082.
[26] M.J. Perez, K. Vergara-Pulgar, C. Jara, F. Cabezas-Opazo, R.A. Quintanilla, Caspase-cleaved tau impairs mitochondrial dynamics in Alzheimer's disease, Mol. Neurobiol. 55 (2) (2018) 1004–1018.
[27] Y. Hu, X.C. Li, Z.H. Wang, Y. Luo, X. Zhang, X.P. Liu, Q. Feng, Q. Wang, Z. Yue, Z. Chen, K. Ye, J.Z. Wang, G.P. Liu, Tau accumulation impairs mitophagy via increasing mitochondrial membrane potential and reducing mitochondrial Parkin, Oncotarget 7 (2016) 17356–17368.
[28] G. Plucinska, D. Paquet, A. Hruscha, L. Godinho, C. Haass, B. Schmid, T. Misgeld, In vivo imaging of disease-related mitochondrial dynamics in a vertebrate model system, J. Neurosci. 32 (2012) 16203–16212.
[29] K. Shahpasand, I. Uemura, T. Saito, T. Asano, K. Hata, K. Shibata, Y. Toyoshima, M. Hasegawa, S. Hisanaga, Regulation of mitochondrial transport and inter-microtubule spacing by tau phosphorylation at the sites hyperphosphorylated in Alzheimer's disease, J. Neurosci. 32 (2012) 2430–2441.
[30] Z. Tang, E. Ioja, E. Bereczki, K. Hultenby, C. Li, Z. Guan, B. Winblad, J.J. Pei, mTor mediates tau localization and secretion: implication for Alzheimer's disease, Biochim. Biophys. Acta 1853 (2015) 1646–1657.
[31] G. Amadoro, V. Corsetti, A. Stringaro, M. Colone, S. D'Aguanno, G. Meli, M. Ciotti, G. Sancesario, A. Cattaneo, R. Bussani, D. Mercanti, P. Calissano, A NH_2 tau fragment targets neuronal mitochondria at AD synapses: possible implications for neurodegeneration, J. Alzheimers Dis. 21 (2010) 445–470.
[32] S. Cabantous, T.C. Terwilliger, G.S. Waldo, Protein tagging and detection with engineered self-assembling fragments of green fluorescent protein, Nat. Biotechnol. 23 (2005) 102–107.
[33] J.D. Pedelacq, S. Cabantous, T. Tran, T.C. Terwilliger, G.S. Waldo, Engineering and characterization of a superfolder green fluorescent protein, Nat. Biotechnol. 24 (2006) 79–88.
[34] T. Cali, D. Ottolini, M.E. Soriano, M. Brini, A new split-GFP-based probe reveals DJ-1 translocation into the mitochondrial matrix to sustain ATP synthesis upon nutrient deprivation, Hum. Mol. Genet. 24 (4) (2015) 1045–1060.
[35] R.A. Quintanilla, T.A. Matthews-Roberson, P.J. Dolan, G.V. Johnson, Caspase-cleaved tau expression induces mitochondrial dysfunction in immortalized cortical neurons: implications for the pathogenesis of Alzheimer disease, J. Biol. Chem. 284 (2009) 18754–18766.
[36] R.A. Quintanilla, R. von Bernhardi, J.A. Godoy, N.C. Inestrosa, G.V. Johnson, Phosphorylated tau potentiates Aβ-induced mitochondrial damage in mature neurons, Neurobiol. Dis. 71 (2014) 260–269.
[37] R.A. Quintanilla, P.J. Dolan, Y.N. Jin, G.V. Johnson, Truncated tau and Abeta cooperatively impair mitochondria in primary neurons, Neurobiol. Aging 33 (619) (2012) e625–e635.
[38] D. Ottolini, T. Cali, M. Brini, Methods to measure intracellular ca(2+) fluxes with organelle-targeted aequorin-based probes, Methods Enzymol. 543 (2014) 21–45.
[39] D. Cieri, M. Vicario, M. Giacomello, F. Vallese, R. Filadi, T. Wagner, T. Pozzan, P. Pizzo, L. Scorrano, M. Brini, T. Cali, SPLICS: a split green fluorescent protein-based contact site sensor for narrow and wide heterotypic organelle juxtaposition, Cell Death Differ. 25 (6) (2018) 1131–1145.
[40] Z. Polianskyte, N. Peitsaro, A. Dapkunas, J. Liobikas, R. Soliymani, M. Lalowski, O. Speer, J. Seitsonen, S. Butcher, G.M. Cereghetti, M.D. Linder, M. Merckel, J. Thompson, O. Eriksson, LACTB is a filament-forming protein localized in mitochondria, Proc. Natl. Acad. Sci. U. S. A. 106 (2009) 18960–18965.
[41] V. Hung, P. Zou, H.W. Rhee, N.D. Udeshi, V. Cracan, T. Svinkina, S.A. Carr, V.K. Mootha, A.Y. Ting, Proteomic mapping of the human mitochondrial intermembrane space in live cells via ratiometric APEX tagging, Mol. Cell 55 (2014) 332–341.
[42] R.A. McCloy, S. Rogers, C.E. Caldon, T. Lorca, A. Castro, A. Burgess, Partial inhibition of Cdk1 in G 2 phase overrides the SAC and decouples mitotic events, Cell Cycle 13 (2014) 1400–1412.
[43] G. Amadoro, V. Corsetti, F. Florenzano, A. Atlante, M.T. Ciotti, M.P. Mongiardi, R. Bussani, V. Nicolin, S.L. Nori, M. Campanella, P. Calissano, AD-linked, toxic NH_2 human tau affects the quality control of mitochondria in neurons, Neurobiol. Dis. 62 (2014) 489–507.
[44] T. Cali, D. Ottolini, M.E. Soriano, M. Brini, A new split-GFP-based probe reveals DJ-1 translocation into the mitochondrial matrix to sustain ATP synthesis upon nutrient deprivation, Hum. Mol. Genet. 24 (2015) 1045–1060.
[45] S. Paillusson, R. Stoica, P. Gomez-Suaga, D.H. Lau, S. Mueller, T. Miller, C.C. Miller, There's something wrong with my MAM; the ER-mitochondria axis and neurodegenerative diseases, Trends Neurosci. 39 (2016) 146–157.
[46] S. Perreault, O. Bousquet, M. Lauzon, J. Paiement, N. Leclerc, Increased association between rough endoplasmic reticulum membranes and mitochondria in transgenic mice that express P301L tau, J. Neuropathol. Exp. Neurol. 68 (2009) 503–514.
[47] A.Y. Abramov, A.V. Berezhnov, E.I. Fedotova, V.P. Zinchenko, L.P. Dolgacheva, Interaction of misfolded proteins and mitochondria in neurodegenerative disorders, Biochem. Soc. Trans. (2017), https://doi.org/10.1042/BST20170024.
[48] L. Ruan, C. Zhou, E. Jin, A. Kucharavy, Y. Zhang, Z. Wen, L. Florens, R. Li, Cytosolic proteostasis through importing of misfolded proteins into mitochondria, Nature 543 (2017) 443–446.
[49] R. Filadi, E. Greotti, G. Turacchio, A. Luini, T. Pozzan, P. Pizzo, Mitofusin 2 ablation increases endoplasmic reticulum-mitochondria coupling, Proc. Natl. Acad. Sci. U. S. A. 112 (2015) E2174–E2181.
[50] T. Calì, D. Ottolini, A. Negro, M. Brini, alpha-Synuclein controls mitochondrial calcium homeostasis by enhancing endoplasmic reticulum-mitochondria interactions, J. Biol. Chem. 287 (2012) 17914–17929.
[51] K.J. De Vos, G.M. Morotz, R. Stoica, E.L. Tudor, K.F. Lau, S. Ackerley, A. Warley, C.E. Shaw, C.C. Miller, VAPB interacts with the mitochondrial protein PTPIP51 to regulate calcium homeostasis, Hum. Mol. Genet. 21 (2012) 1299–1311.